Journal of Physics: Conference Series

Microwave investigation of pinning in Te- and cubic-BN- added MgB_2

Journal of Physics: Conference Series **1559** (2020) 012039 doi:10.1088/1742-6596/1559/1/012039

Microwave investigation of pinning in Te- and cubic-BN- added MgB_2

A. Alimenti[1], K. Torokhtii[1], M. Grigoroscuta[2], P. Badica[2], A. Crisan[2], E. Silva[1], N. Pompeo[1]

[1]Department of Engineering, Università Roma Tre, Via Vito Volterra 62, Roma 00146, Italy
[2]National Institute of Materials Physics, 405A Atomistilor Street, 077125 Magurele, Romania

E-mail: andrea.alimenti@uniroma3.it

Abstract. MgB_2 has great potential for many applications, thanks to its relatively high critical temperature and low fabrication cost. Large efforts are done to improve the current carrying capabilities of bulks and tapes in view of different application fields, e.g. with the addition of Te and cubic-BN to MgB_2. To elucidate the vortex pinning physics exploiting a different dynamic regime, we present here a microwave study of the pinning properties of spark plasma sintered bulk MgB_2 with and without the addition of 0.01 % at. Te or cubic-BN. We show the surface resistance R_s of the MgB_2 samples measured with a dielectric-loaded resonator at $\sim$ 16.5 GHz and $\sim$ 26.7 GHz in the 10 K-Tc temperature range at fields up to 1.0 T. Then, the MgB_2 R_s is studied with high frequency vortex motion models in order to obtain the pinning constant (Labusch parameter) and the depinning frequency. Finally, the microwave behavior of MgB_2 in the mixed state is compared with the recent results obtained on Nb_3Sn.

1. Introduction

Magnesium diboride (MgB_2) is one of the most technologically interesting superconductor (SC) thanks to its superconductive performances [1] and relatively low fabrication costs [2]. For this reason, different preparation procedures, also with impurities additions, are under investigation to tailor the physical properties of MgB_2 to the new applications requirements. As example, it has been noticed that bulk MgB_2 samples with higher density and a controlled fine particles microstructure exhibit higher critical currents J_c. This effect is due to the grain boundaries pinning contribution in MgB_2 [3]. Thus, fabrication techniques working at high temperatures and high pressures, as the hot pressing [4, 5] or the spark plasma sintering (SPS) [6, 7], are particularly promising. Besides the different fabrication techniques, interesting results are also given working on the chemical composition. Particularly enhanced current carrying capabilities were obtained adding Te or BN based impurities [8–10].

Several characterization methods, in addition to the more common dc-techniques, were used to investigate the MgB_2 low temperature behavior [11,12]. In particular, since the very same year (2001) of the discovery of superconductivity in MgB_2, the microwave (μw) surface resistance R_s of this SC has been studied [12–14]. Microwave characterization techniques have in fact always been particularly interesting for matter physics experimental studies since they provide different and complementary information with respect to those given by dc characterization methods [15]. Moreover, the study of the MgB_2 at μw, and in high externally applied magnetic fields, recently became particularly requested, since MgB_2 is a possible material candidate for the realization

of SC cavities for axions detection [16]. Thus, μw experimental studies on MgB_2 in the mixed state [17–19] are requested both for their contribution to fundamental physics investigations, particularly from the point of view of multi band SC, but also for technological applications.

In this framework, with this work, we want to explore the vortex motion regime, at high frequency, of different MgB_2 samples. In particular, we will study the microwave response of bulk MgB_2 samples, prepared with the SPS technique, with and without the addition of 0.01 % at. Te ($MgB_2(Te)_{0.01}$) or cubic-BN ($MgB_2(c\text{-}BN)_{0.01}$). These samples have been chosen for their good performances in high magnetic fields [8–10]. Here, we present measurements of MgB_2 surface resistance R_s performed in an applied magnetic field. The R_s is measured with a bi-tonal dielectric loaded resonator working at 16.5 GHz and 26.7 GHz at low μw power in order to firmly remain in the R_s linear regime. The results are shown in this work and compared with R_s of Nb_3Sn.

We propose a physical analysis of the measured R_s in order to obtain the de-pinning frequency ν_p and the Labusch parameter k_p of MgB_2. ν_p represents the frequency above which the vortices start oscillating in phase with the electromagnetic field excitation. Thus, it is a cross–over frequency between an elastic and a pure dissipative vortex motion. ν_p is an interesting design parameters for perspective high frequency applications of MgB_2 as the axions cavities [20]. Then, the pinning constant or Labusch parameter k_p is a measure of the pinning strength, or in other terms of the pinning potential wells steepness. Its amplitude and field dependence can give information about the effective pinning phenomena in MgB_2.

The paper is organized as follows. In Sec. 2 we present the physical models used for the R_s data elaboration. Then, in Sec. 3 the measurement technique is presented and finally in Sec. 4 the results are discussed.

2. Surface resistance in the mixed state

At μw frequencies the physical quantity usually used to characterize good conductors materials is the surface impedance $Z_s = R_s + \mathrm{i}X_s$, with R_s the surface resistance and X_s the surface reactance. With classical electrodynamics the surface impedance of bulk conducting materials (i.e. samples several times thicker than the characteristics screening lengths), in the local limit, is expressed by $Z_s = \sqrt{\mathrm{i}\omega\mu_0\tilde{\rho}}$ [21], where $\omega = 2\pi\nu$ is the measurement angular frequency, μ_0 the vacuum magnetic permeability and $\tilde{\rho}$ a complex resistivity which includes all the dissipative and energy storing phenomena into the material. In SC materials in the mixed state $\tilde{\rho}$ includes the contribution of both the super/normal-fluid and the vortex motion.

At these frequencies, the standard model used to describe the interaction between moving vortices with the superconductive currents is the Coffey-Clem model (CC) [22]. However, the validity of the CC model is not granted in dual or multi band SCs, as in case of MgB_2. This is because the interaction between the different supercurrents families with the composite fluxons can be particularly troublesome to be simply modeled. For this reason, we reduce our investigation only at relatively high magnetic field where the superconducting weak π-band is completely suppressed [19, 23]. Thus, the $\tilde{\rho}$ is described with the CC model as:

$$\tilde{\rho} = \frac{\tilde{\rho}_{vm} + \mathrm{i}/\sigma_2}{1 + \mathrm{i}\sigma_1/\sigma_2} \,, \tag{1}$$

where $\tilde{\rho}_{vm}$ is the vortex motion complex resistivity and σ_1 and σ_2 the real and the imaginary part of the complex conductivity of the SC. In dual band SCs with weak intraband scattering, as in MgB_2 [24, 25], the two fluids (2F) model conductivity $\tilde{\sigma}_{2F}$ can be generalized as $\tilde{\sigma}_{2F} = \sigma_1 + \mathrm{i}\sigma_2 = (\sigma_{1,\sigma} + \sigma_{2,\pi}) - \mathrm{i}(\sigma_{2,\sigma} + \sigma_{2,\pi})$ [19]. σ_1 and σ_2 are the real and imaginary part of the overall $\tilde{\sigma}_{2F}$. In the low frequency limit, $\sigma_{1,\sigma}$, $\sigma_{1,\pi}$ are the conductivity of the normal fluid of the σ and π bands respectively while $\sigma_{2,\sigma}$, $\sigma_{2,\pi}$ are those of the superfluid of the two bands.

At sufficiently high excitation frequencies we can treat the vortex lattice as composed by individual and non interacting vortices in the small oscillation regime. Thus, $\tilde{\rho}_{vm}$ can be obtained starting from the dynamic equation of the forces acting on a single fluxon. Neglecting thermal effects, the only forces applied to a moving fluxon are the Lorentz driving force generated by the induced μw currents $J_{\mu w}$, the viscous drag force, with drag coefficient η, related to the quasiparticles relaxation processes and finally the pinning elastic force $k_p x$. Thus, the pinning constant k_p represents the elastic constant and x the vortex displacement around the pinning centre. Solving the dynamic equation for a non massive fluxon brings to the $\tilde{\rho}_{vm}$ of the Gittleman–Rosenblum model (GR) [26]:

$$\tilde{\rho}_{vm} = \frac{\Phi_0 B}{k_p} \frac{2\pi}{1/\nu_p - \mathrm{i}/\nu} \,. \tag{2}$$

In eq. (2) we have used $\eta = k_p/(2\pi\nu_p)$ to highlight the pinning frequency ν_p. Finally, it must be remembered that the GR model is valid only for negligible thermal effects (i.e. no thermal creep). However, at low enough temperature and field, the regime of interest here, it is safe to assume that creep does not take a prominent role, also in view of the analysis in [27]. In any case, neglecting the creep altogether in the analysis gives at worst a lower bound for ν_p and k_p [27].

3. Measurement technique

The measurement of the surface resistance R_s of conductive materials with dielectric loaded resonators (DR) is a well known technique particularly reliable also with SC samples due to its high sensitivity [28]. The dielectric crystal is held between the two bases of the metallic cavity. In this way both a reduction of the resonator dimensions (useful to fit with the cryostat bore) and a reduction of the conduction losses on the lateral wall of the DR are obtained. This last feature increases the quality factor Q of the resonator hence the measurement sensitivity.

We use an end-wall replacement configuration, loading the flat SC sample into the resonating cavity in order to substitute a base of the DR itself. Q is related to the surface resistance of the SC sample $R_{s,SC}$ by:

$$\frac{1}{Q} = \frac{R_{s,SC}}{G_s} + background \,, \tag{3}$$

where G_s is a geometrical factor evaluated with e.m. simulations and *background* is the contribution of all the other components of the DR to the measured Q. $R_{s,SC}$ is obtained subtracting from eq. (3) $1/Q$ measured with no sample loaded into the DR with the calibration procedure described in [29].

Our measurement set-up is composed by a bi-tonal cylindrical DR made of OFHC copper, loaded with a sapphire single-crystal (height $h = 4.50$ mm, diameter $\varnothing = 7.13$ mm). The DR is used at $\sim$ 16.5 GHz and $\sim$ 26.7 GHz corresponding to the e.m. resonance modes TE_{011} and TE_{021}. With a Vector Network Analyzer the scattering (S) parameters of the two modes are acquired. Then, the loaded quality factor Q_l is obtained fitting the complex transmission S-parameters with modified Lorentzian curves [29] and the unloaded $Q = Q_l(1+\beta)$ is obtained by measuring the coupling coefficient β with the procedure used in the TMQF algorithm [30] applied to the reflection S-parameters.

All the measurements are performed in field cooling conditions and slowly rising the temperature at 0.1 K/min after the thermalization at the lowest temperature in a helium flow cryostat. The magnetic field is generated with an electromagnet and applied perpendicularly to the surface of the sample.

We measured three MgB_2 bulk samples made with the spark plasma sintering technique (SPS): pristine MgB_2, MgB_2 +0.01 % at. Te ($MgB_2(Te)_{0.01}$) and MgB_2 +0.01 % at. c-BN

$(MgB_2(c\text{-}BN)_{0.01})$. Samples preparation techniques and their characterization with electric, magnetic, X-ray and microscopic methods are well described elsewhere [7–10].

4. Results

We present in this section the obtained results. We firstly show the measured R_s of the three samples. Then, we analyze the R_s with the physical models previously discussed to obtain the vortex motion parameters in MgB_2. These are commented and compared to those of Nb_3Sn.

4.1. Surface resistance

The measured R_s at 16.5 GHz and 26.7 GHz, of the three MgB_2 samples, are shown in Figure 1 and Figure 2 respectively. The shown R_s are measured at $\mu_0 H = \{0, 0.5, 1.0\}$ T. We observed that the addition of Te or c-BN does not degrade the T_c as confirmed in [8–10] but rather it slightly enhances T_c. On the contrary, the pristine one exhibits a lower normal state surface resistance $R_{s,n}$ than those of the other samples: this can be related to the increased grain boundaries interfaces number and disorder induced by the Te and c-BN additions [8–10]. Then,

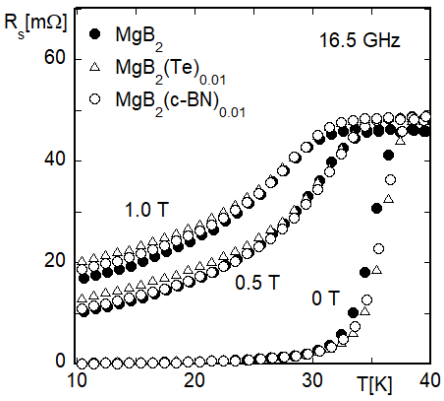

Figure 1. The surface resistance R_s of the three MgB_2 samples measured at 16.5 GHz and $\mu_0 H = \{0, 0.5, 1.0\}$ T.

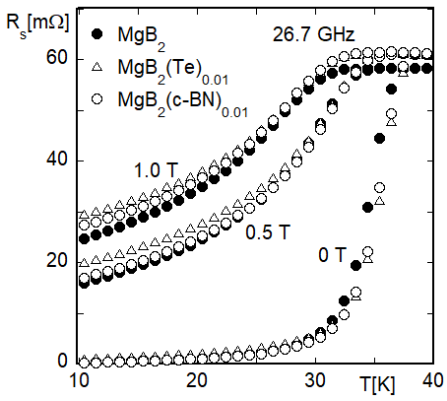

Figure 2. The surface resistance R_s of the three MgB_2 samples measured at 26.7 GHz and $\mu_0 H = \{0, 0.5, 1.0\}$ T.

when a magnetic field is applied, R_s correctly increases because of the vortex motion energy dissipation and storing phenomena contribution. The in field behavior of the three samples is almost indistinguishable at this low applied magnetic field. In fact, as shown in [8–10], the superconductive performances enhancements due to the addition of Te or c-BN are mostly evident at higher fields, above ~ 5 T. Anyway, we can notice that the $MgB_2(Te)_{0.01}$ sample shows a slightly higher R_s than the $MgB_2(c\text{-}BN)_{0.01}$ and the pristine samples. The same behavior is shown at both frequencies. We will show later that the Te or c-BN additions have no influence on ν_p, which comes out to be almost the same in all samples.

As a comparison, $R_s(10\,\mathrm{K}, 1\,\mathrm{T}) \simeq 16\ \mathrm{m\Omega}$ measured on the pristine MgB_2 sample at 16.5 GHz is almost the same of that shown by Nb_3Sn in similar conditions [31]. However, it should be noticed that the normal state surface resistance of the two SCs is $R_{s,n,MgB_2} \simeq 46\ \mathrm{m\Omega}$ for pristine MgB_2 and $R_{s,n,Nb_3Sn} \simeq 93\ \mathrm{m\Omega}$ for Nb_3Sn. Thus, at 10 K with just 1 T applied, R_s of MgB_2 is the 35 % of R_{s,n,MgB_2} while for Nb_3Sn R_s is the 17 % of its normal state value. The relatively sharp increase of the MgB_2 surface resistance with the applied magnetic field is due to the π-band suppression, thus to the anomalous field dependence of the flux-flow resistivity in this superconductor [17,32,33] with respect to the conventional Bardeen-Stephen behavior in Nb_3Sn.

4.2. Pinning parameters

We now apply the physical models introduced in Sec. 2 to R_s measurements. Despite the complexity of the models, particularly increased by the double SC band, we firstly show how ν_p and k_p are estimated starting from only two independent experimental determination (i.e. R_s at two different frequencies) and working with a six free parameters model (i.e. $\sigma_{1,\sigma}$, $\sigma_{2,\sigma}$, $\sigma_{1,\pi}$, $\sigma_{2,\pi}$, ν_p and k_p). The possible values spaces of the four normal/super-fluid conductivities are reduced with physical constraints and literature values. The obtained variability intervals are then propagated into the models as uncertainties. We show how the relatively large interval of the unknown conductivity parameters slightly affects the pinning parameter evaluation which can therefore be considered reliable.

To obtain ν_p and k_p we numerically solve the system of two equations $\Re\{\sqrt{\mathrm{i}\omega_1\mu_0\tilde{\rho}(\omega_1)}\} = R_{s,\omega_1}$ and $\Re\{\sqrt{\mathrm{i}\omega_2\mu_0\tilde{\rho}(\omega_2)}\} = R_{s,\omega_2}$, where $\omega_1/(2\pi) = 16.5$ GHz, $\omega_2/(2\pi) = 26.7$ GHz and R_{s,ω_1}, R_{s,ω_2} are the R_s measured at the two frequencies. We put eq. (1) in $\tilde{\rho}$ using the GR model for $\tilde{\rho}_{vm}$ (eq. (2)). Then, with the two fluid generalized model (2F) for dual band SCs, the complex conductivity is described as $\tilde{\sigma}_{2F} = (\sigma_{1,\sigma} + \sigma_{2,\pi}) - \mathrm{i}(\sigma_{2,\sigma} + \sigma_{2,\pi})$. Above 0.5 T and 10 K, the superconductive π-band is assumed to be almost suppressed [19], thus $\sigma_{2,\pi} = 0$ and $\sigma_{1,\pi} = \sigma_{n,\pi}$. Moreover, since the maximum measurement field is $\mu_0 H = 1$ T and $\mu_0 H_{c2}(0) \sim 15$ T, the σ-band is still far from its critical surface, then $\sigma_{1,\sigma} \ll \sigma_{1,\pi}$, $\sigma_1 \simeq \sigma_{n,\pi}$ and $\tilde{\sigma}_{2F} \simeq \sigma_{n,\pi} - \mathrm{i}\sigma_{2,\sigma}$. Since in this work we are interested in the evaluation of the pinning parameters and since we do not have independent measurements of $\sigma_{n,\pi}$ and $\sigma_{2,\sigma}$, we let them vary in their whole span of values found in literature [19, 33]. Then, we propagate the variability on $\sigma_{n,\pi}$ and $\sigma_{2,\sigma}$ as uncertainties on these parameters. For the $\sigma_{n,\pi}$ we start from the normal state resistivity $\rho_n = 2R_{s,n}^2/(\omega\mu_0) \simeq 3.3\ \mu\Omega$cm which is obtained by the normal state surface resistance $R_{s,n}$ above T_c. Then, with the measured $\rho_n = 1/(\sigma_{n,\pi} + \sigma_{n,\sigma})$ and knowing that $0.25 < \sigma_{n,\sigma}/\sigma_{n,\pi} < 0.5$ from literature [19, 33], we obtain 20.2 MS/m $< \sigma_{n,\sigma} <$ 24.2 MS/m. Whereas, since $\sigma_{2,\sigma} = 1/(\omega\mu_0\lambda^2)$, with λ the London penetration depth, we use literature λ values 85 nm $< \lambda(0) <$ 180 nm [34] for $\sigma_{2,\sigma}$ evaluation. In our reduced temperature span the $\lambda(T)$ temperature dependence can be neglected in a first approximation. Thus we consider $\lambda(T)$ constant and we use $\lambda = 150$ nm as an estimation. However, it must be noticed that letting $\sigma_{n,\pi}$ and $\sigma_{2,\sigma}$ vary in their literature intervals does not drastically change the resulting evaluation since it causes only a 7 % of maximum error on ν_p and k_p. The obtained ν_p and k_p are shown in Figure 3 and Figure 4.

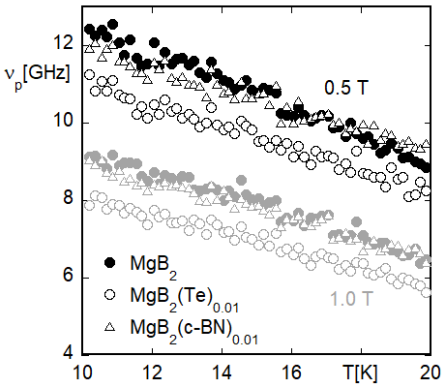

Figure 3. The measured de–pinning frequency ν_p of the three MgB_2 samples at 0.5 T (black symbols) and 1 T (gray symbols).

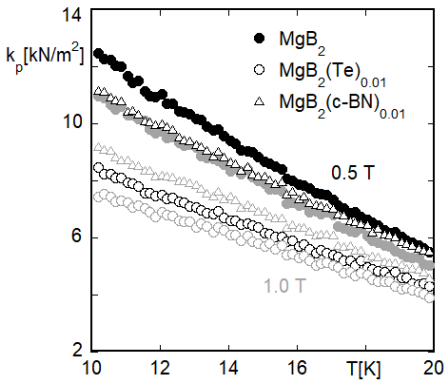

Figure 4. The measured Labusch parameter k_p of the three MgB_2 samples at 0.5 T (black symbols) and 1 T (gray symbols).

We show in Figure 3 the measured ν_p of the three samples at 0.5 T and 1.0 T. ν_p of the pristine

samples and that of MgB_2(c-BN)$_{0.01}$ are the same, while Te additions lower ν_p somewhat. The measured ν_p on pristine MgB_2 is well in agreement with other literature results [18, 19]. The ν_p values are relatively high in MgB_2, higher than that observed on Nb_3Sn, for which at low field $\mu_0 H < 2$ T and low temperature < 12 K, the ν_p saturates at ~ 7 GHz [31]. However, the MgB_2 ν_p seems strongly dependent on the applied magnetic field, in fact at 10 K it decreases from ~ 12 GHz to ~ 9 GHz upon increasing the applied magnetic field from 0.5 T to 1 T. On the other hand, in Nb_3Sn ν_p is almost constant at low temperature up to 8 T. This suggests that at higher magnetic fields Nb_3Sn can exhibit better high frequencies performances with respect to MgB_2. Thus, depending on the working conditions one SC could be more or less convenient than the other for radio frequencies applications. Moreover, ν_p and k_p field dependencies (see Figure 4) indicate that even at this low magnetic field values the effective pinning potential depends on the magnetic field. This suggests that collective pinning acts in MgB_2 as confirmed also by [18]. The Labusch parameter measured on the three samples is highest in the pristine MgB_2 but its percentage temperature variation is greater than what observed in the doped samples: with respect to their values at 10 K and 0.5 T, the k_p of the three samples are reduced at 20 K and 0.5 T by the 57 %, the 52 % and the 50 % respectively for the pristine one, the Te and the c-BN added samples. Since k_p can be related to the maximum force acting on a fluxon, thus to an effective critical current, this different temperature dependence suggests that at higher temperature or higher fields the MgB_2(Te)$_{0.01}$ and MgB_2(c-BN)$_{0.01}$ could exhibit better pinning performances than the pristine MgB_2 also at high frequency, similarly to the higher fields observations by dc measurements [8–10].

5. Conclusion

We presented and compared the measurements of the surface resistance R_s of three bulk MgB_2 samples made with the spark plasma sintering technique with and without the addition of 0.01 % at. Te or cubic-BN. The measurements were performed with a bi-tonal dielectric loaded resonator at 16.5 GHz and 26.7 GHz and with applied magnetic field $\mu_0 H = \{0, 0.5, 1.0\}$ T in field cooling conditions.

Because of the weak intraband scattering in MgB_2, it was possible to extract useful information about vortex motion in this SC from R_s. In particular, we obtained the de-pinning frequency ν_p and the Labusch parameter k_p using the generalized two fluid model [19] and describing the vortex motion resistivity with the standard Glitteman–Rosenblum model [26]. The obtained results on the pristine sample are in agreement with other literature experimental studies [18, 19]. Thus, we compare the pristine MgB_2 sample with those with Te and c-BN additions. It is shown that these impurities do not alter significantly the high frequency pinning properties of MgB_2. In particular the MgB_2(c-BN)$_{0.01}$ sample shows performances closer to the pristine than what the MgB_2(Te)$_{0.01}$ does. The ν_p at 0.5 T and 10 K is about 12 GHz but at 1 T and at the same temperature it is sharply reduced by about the 30 %. This strong field dependence of ν_p, reported in films [18], suggests the importance of collective pinning in MgB_2.

Since the Te and c-BN additions are shown to enhance the critical current of MgB_2 particularly at high fields, further microwave measurements would be useful to be performed above 1 T to better understand the reasons of this enhancement.

Acknowledgment

Authors from Romania acknowledge UEFISCDI, POC 37_697 No. 28/01.09.2016. Authors also thank Dr. M. Burdusel and Dr. G. Aldica for assistance with sample preparation.

References

[1] Nagamatsu J, Nakagawa N, Muranaka T, Zenitani Y and Akimitsu J 2001 *Nature* **410** 63
[2] Cooley L, Ghosh A and Scanlan R 2005 *Supercond Sci Technol* **18** R51

[3] Larbalestier D *et al.* 2001 *Nature* **410** 186
[4] Tampieri A, Celotti G, Sprio S, Caciuffo R and Rinaldi D 2004 *Physica C: Supercond* **400** 97–104
[5] Kováč P, Hušek I, Melišek T, Fedor J, Cambel V, Morawski A and Kario A 2009 *Physica C: Supercond* **469** 713–716
[6] Dancer C, Prabhakaran D, Başoğlu M, Yanmaz E, Yan H, Reece M, Todd R and Grovenor C 2009 *Supercond Sci Technol* **22** 095003
[7] Aldica G, Batalu D, Popa S, Ivan I, Nita P, Sakka Y, Vasylkiv O, Miu L, Pasuk I and Badica P 2012 *Physica C: Supercond* **477** 43–50
[8] Sandu V, Aldica G, Popa S, Enculescu M and Badica P 2016 *Supercond Sci Technol* **29** 065012
[9] Badica P, Aldica G, Burdusel M, Popa S, Negrea R, Enculescu M, Pasuk I and Miu L 2014 *Supercond Sci Technol* **27** 095013
[10] Aldica G, Popa S, Enculescu M and Badica P 2012 *Scripta Mater* **66** 570–573
[11] Shields T, Kawano K, Holdom D and Abell J 2002 *Supercond Sci Technol* **15** 202
[12] Zhukov A, Cohen L, Yates K, Perkins G, Bugoslavsky Y, Polichetti M, Berenov A, Driscoll J M, Caplin A, Hao L *et al.* 2001 *Supercond Sci Technol* **14** L13
[13] Purnell A, Zhukov A, Nurgaliev T, Lamura G, Bugoslavsky Y, Lockman Z, MacManus-Driscoll J, Zhai H, Christen H, Paranthaman M *et al.* 2002 *Supercond Sci Technol* **16** 1
[14] Oates D, Agassi Y and Moeckly B 2010 *Supercond Sci Technol* **23** 034011
[15] Pompeo N, Augieri A, Torokhtii K, Galluzzi V, Celentano G and Silva E 2013 *Appl Phys Lett* **103** 022603
[16] Kuzmin L S, Sobolev A S, Gatti C, Di Gioacchino D, Crescini N, Gordeeva A and Il'ichev E 2018 *IEEE Trans Appl Supercond* **28** 1–5
[17] Shibata A, Matsumoto M, Izawa K, Matsuda Y, Lee S and Tajima S 2003 *Phys Rev B* **68** 060501
[18] Zaitsev A, Schneider R, Hott R, Schwarz T and Geerk J 2007 *Phys Rev B* **75** 212505
[19] Sarti S, Amabile C, Silva E, Giura M, Fastampa R, Ferdeghini C, Ferrando V and Tarantini C 2005 *Phys Rev B* **72** 024542
[20] Gioacchino D *et al.* 2019 *IEEE Trans Appl Supercond* **29** 1–5
[21] Jackson J D 1999 *Classical Electrodynamics* (John Wiley & Sons)
[22] Coffey M W and Clem J R 1991 *Phys Rev Lett* **67** 386
[23] Bugoslavsky Y, Miyoshi Y, Perkins G, Caplin A, Cohen L, Pogrebnyakov A and Xi X 2004 *Phys Rev B* **69** 132508
[24] Mazin I, Andersen O, Jepsen O, Dolgov O, Kortus J, Golubov A A, Kuz'menko A and Van der Marel D 2002 *Phys Rev Lett* **89** 107002
[25] Gozzelino L, Minetti B, Ummarino G, Gerbaldo R, Ghigo G, Laviano F, Lopardo G, Giunchi G, Perini E and Mezzetti E 2009 *Supercond Sci Technol* **22** 065007
[26] Gittleman J I and Rosenblum B 1966 *Phys Rev Lett* **16** 734
[27] Pompeo N and Silva E 2008 *Phys Rev B* **78** 094503
[28] Mazierska J 1997 *J Supercond* **10** 73–84
[29] Alimenti A, Torokhtii K, Silva E and Pompeo N 2019 *Meas Sci Technol* **30** 065601
[30] Leong K and Mazierska J 2001 *J Supercond* **14** 93–103
[31] Alimenti A, Pompeo N, Torokhtii K, Spina T, Flükiger R, Muzzi L and Silva E 2019 *IEEE Trans Appl Supercond* **29** 1–4
[32] Silaev M and Vargunin A 2016 *Phys Rev B* **94** 224506
[33] Goryo J and Matsukawa H 2005 *J Phys Soc Jpn* **74** 1394–1396
[34] Buzea C and Yamashita T 2001 *Supercond Sci Technol* **14** R115